Marine Pollution Bulletin 139 (2019) 214–220

Contents lists available at ScienceDirect

Marine Pollution Bulletin

journal homepage: www.elsevier.com/locate/marpolbul

Sinking velocity of sub-millimeter microplastic

David Kaiser*, Arne Estelmann, Nicole Kowalski, Michael Glockzin, Joanna J. Waniek

Leibniz Institute for Baltic Sea Research Warnemünde, Seestraße 15, 18119 Rostock, Germany

ARTICLE INFO

Keywords:
Microplastic
Sub-mm particle size
Terminal sinking velocity
Shadowgraphy
Settling experiments

ABSTRACT

Sinking experiments were conducted using irregularly shaped polyamide (PA), polymethyl methacrylate (PMMA), and polyethylene terephthalate (PET) particles sized 6 to 251 µm. Certified PS spheres were used to validate experiments and showed that the effect of particle size on terminal sinking velocity is well reproduced by the method. As expected sinking velocities of irregularly shaped particles were considerably lower than theoretical values for spheres of the same size range calculated via several approximations available in the literature. Despite the influence of particle shape, the dependence of terminal sinking velocity on particle size can reasonably well be described by a quadratic linear regression, with an average determination of 63%. To generalize results we present a model that predicts terminal sinking velocity as a function of particle size and particle excess density over the fluid. Improving the predictive power of this model requires further experiments with a range of particle characteristics.

1. Introduction

Plastic pollution is now firmly recognized as one of the major and most visible anthropogenic fingerprints on aquatic environments. Despite numerous government and private sector interventions (on plastic use), plastic production continues to increase and in the first 10 years of the twentyfirst century approached the total production in the twentieth century (Thompson et al., 2009). Much of the plastic in aquatic environments is small in size, with polymer particles < 5 mm usually defined as microplastic (e.g. da Costa et al., 2016; Hidalgo-Ruz et al., 2012). Sub-mm microplastic, particles with at least one dimension being smaller than 1 mm, contribute a large proportion to the abundance of microplastic in surface waters of the world oceans (Cózar et al., 2014; Lenz et al., 2016), the Mediterranean Sea (Cózar et al., 2015), surface waters of the western Canadian coast and the north eastern Pacific Ocean (Desforges et al., 2014), and the north Pacific Central Gyre (Moore et al., 2001). Within the sub-mm size class there appears to be a decrease in abundance of the smallest particles (Cózar et al., 2015; Desforges et al., 2014; Moore et al., 2001). The fragmentation of larger plastic debris causes an exponential increase in the abundance of smaller, secondary, microplastic particles (see e.g. Lenz et al., 2016). Primary sources of sub-mm microplastic include care products such as hand, face and contact lens cleaners, and tooth paste, as well as fresh and used air-blast cleaning media, plasticizing material and raw plastic feed stock (Gregory, 1996; Pinto da Costa et al., 2016). Such particles eventually reach the marine environment via waste water, which contains microplastic regardless of filtration treatment level (Sutton et al., 2016). Microplastic present in the environment is inadvertently but inevitably ingested by living organisms, and sub-mm microplastic is frequently found in benthic and demersal organisms in nature (Van Cauwenberghe et al., 2015; Bellas et al., 2016; Browne et al., 2008), where they can cause decreased food ingestion, fecundity and survival of the organism (Cole et al., 2015). The consumption of contaminated seafood may cause humans to ingest 11,000 particles per annum (Van Cauwenberghe and Janssen, 2014). Much of the microplastic introduced into the marine environment eventually deposits in sediments from beaches to the deep sea (e.g. Claessens et al., 2011; Browne et al., 2010; Van Cauwenberghe and Janssen, 2014; Van Cauwenberghe et al., 2015; Woodall et al., 2014; Fischer et al., 2015). The transport of microplastic to the sediments is not yet well understood, but its presences throughout the water column (Doyle et al. 2011; Courtene-Jones et al., 2017; Bagaev et al., 2017; Kanhai et al. 2018) suggests that free vertical sinking of individual particles is an important mechanism. At least some of these particles are intrinsically negatively buoyant, e.g. polyesters (Woodall et al., 2014). Thus, the terminal sinking velocity, i.e. the velocity a sinking particle assumes when its gravitational acceleration is balanced by the drag force acting on the particle as a function of the particles properties as well as the properties of the surrounding medium, is a major component in the transport and fate of negatively buoyant microplastic (Chubarenko et al., 2016; Zhang, 2017; Khatmullina and Isachenko, 2017). Numerous formulae have been developed to predict a particle's terminal

* Corresponding author.
E-mail address: david.kaiser@io-warnemuende.de (D. Kaiser).

https://doi.org/10.1016/j.marpolbul.2018.12.035
Received 17 August 2018; Received in revised form 14 December 2018; Accepted 14 December 2018
Available online 29 December 2018

sinking velocity, and their applicability has been repeatedly tested for particles with different sets of properties (e.g. Zhiyao et al., 2008; Camenen, 2007), including differently shaped microplastic particles (Kowalski et al., 2016; Khatmullina and Isachenko, 2017). While the terminal sinking velocity of regularly shaped microplastic particles can be accurately predicted via existing semi-empirical parametrizations (Khatmullina and Isachenko, 2017), such predictions underestimate the terminal sinking velocity of irregularly shaped microplastic particles (Kowalski et al., 2016). Microplastic particle properties (e.g. particle density, shape and size range) are expected to cause different behavior than observed for natural particles (Kooi et al., 2018; Zhang, 2017). Recently transport simulations have included results from experimental sinking studies to improve backtracking source appointment of microplastic in the marine environment (Bagaev et al., 2017; Liubartseva et al., 2018). Thus, the availability of empirical data on the sinking behavior of microplastic particles is a prerequisite for the parametrization of microplastic transport in models.

In order to provide applicable data on the terminal sinking velocity of irregularly sub-mm microplastic particles, we conducted laboratory experiments using negatively buoyant particles ≤251 μm. We hypothesized that terminal sinking velocity would negatively deviate from theoretical calculations but would be sufficiently predictable from particle properties like size and density.

2. Material and methods

2.1. Particle terminal sinking velocity

Microplastic particle sinking was recorded using the shadowgraphy method described in detail by Glockzin et al. (2014), who present a schematic picture of the experimental setup used in this study. Here, a micro camera recorded the trajectory of a back-lit particle through a sealed photometric cuvette (10 × 10 × 150 mm) jacketed by a water chamber for temperature control (100 mm high, 50 mm edge length, 1 mm wall thickness). Temperature in the water jacket was continuously logged and during the experiments was 19.44 ± 0.55 °C. Ambient air temperature was stabilized at 20 °C by the laboratory air conditioning unit. To minimize electrostatic charge, microplastic particles were stored in due experimental water before being transferred into the cuvette as a suspension using a Pasteur pipette protruding through the cuvette's top seal. To simulate sinking in different aquatic environments, the cuvette was filled with filtered (0.7 μm nominal pore size GF/F) water of salinity 0 (deionized water; 998 kg m^{-3}), 15 (Baltic Sea water; 1010 kg m^{-3}) or 36 (North Atlantic seawater; 1026 kg m^{-3}). The polymers polyamide (PA), polymethyl methacrylate (PMMA), and polyethylene terephthalate (PET) were used in this experiment because, with densities of 1140, 1190, and 1390 kg m^{-3}, respectively, these high density plastics natively travel through the water column and reach the bottom. From virgin pallets of these polymers, obtained from different suppliers (see Kowalski et al., 2016), sub-mm particles were produced by comminution at the Department of Mineral Processing of the Brandenburg University of Technology Cottbus-Senftenberg (BTU), using an ultracentrifuge mill (ZM 200) in combination with a CryoMill (both Retsch GmbH, Germany) under continuous liquid nitrogen cooling to enhance brittleness and avoid melting of the plastics. This process fragments particles without changing their physical and chemical properties.

Particle sinking was recorded either as still image intervals or as videos from which still images were extracted in 1 second intervals. The camera was not moved during the registration of an individual particle's sinking process, which was recorded for durations between 3 and 179 s, depending on the velocity of the particle. Individual shadowgraphs of one particle were combined using ImageJ (https://imagej.net) to produce one image file containing the sinking sequence. Terminal sinking velocity w_s was calculated using a MATLAB routine (Glockzin et al., 2014). On the sinking sequence image file, the distance between intervals was measured and converted to sinking velocity under consideration of the image resolution and time lap between intervals. The MATLAB routine was also used to measure the longest and shortest axes of each particle. This was used to calculate particle size expressed as equivalent spherical diameter (ESD) (e.g. Kumar et al., 2010):

$$ESD = (AC^2)^{1/3}, \tag{1}$$

where A and C are the measured major (i.e. longest) and minor (i.e. shortest) axes of the particle.

To avoid effects of convection influencing the results, particles were excluded from analyses if the sequence image showed deviation from vertical sinking ≥10°, or if the location of particles along the sinking sequence indicated variable or interrupted sinking. Equal distances of particle shadows between time steps of the sequence also show that the particle reached terminal sinking velocity, i.e. did not further accelerate along the sequence. The sinking velocity of particles is strongly influenced by the presence of other particles (e.g. Cheng, 1997). Even at low concentrations, this can lead to a significant reduction in sinking velocity of individual particles (Baldock et al., 2004). In order to avoid hindered sinking, particles were excluded from analyses if more than one particle was visible in the sequence. For better comparability, w_s was standardized to 20 °C, using the ratio of the particle's theoretical w_s after Stokes at measured temperature and at 20 °C as a factor applied to measured w_s of the particle at measured temperature. In bounded space w_s is reduced by the backflow effect along the boundaries of the container, and a wall correction factor was applied to compensate for this effect (Ristow, 1997):

$$\frac{w_s(D/L)}{w_s^{\infty}} \approx \left(1 - 1.14\frac{D}{L}\right), \tag{2}$$

where $w_s(D/L)$ is the velocity of a particle with size D in a space bound by length scale L and w_s^{∞} the unbounded velocity of the same particle. Temperature and wall effect corrections led to an average increase in w_s of 2.2%. The following section reports and discusses corrected sinking velocities. The statistical distribution of the particles' three dimensional shape characteristics was calculated for a subset of particles for which rotation during sinking allowed views from several directions (n = 689). The length scales of the major (A), intermediate (B) and minor (C) axes were used to calculate the eccentricity,

$$e = \sqrt{1 - \frac{C^2}{A^2}}, \tag{3}$$

sphericity following Krumbein (1941)

$$\psi = \left(\frac{BC}{A^2}\right)^{1/3}, \tag{4}$$

sphericity following Sneed and Folk (1958)

$$\psi_p = \left(\frac{A^2}{AB}\right)^{1/3}, \tag{5}$$

flatness following Cailleux (1945)

$$F = \left(\frac{A+B}{2C}\right), \tag{6}$$

the Corey shape factor (e.g. Komar, 1980)

$$CSF = \frac{C}{\sqrt{BA}}, \tag{7}$$

and Janke's shape factor E (e.g. Komar, 1980)

$$E = C\left[\frac{C^2 + B^2 + A^2}{3}\right]^{-1/2}. \tag{8}$$

The Reynolds number Re was calculated as

$$Re = \frac{w_s L}{\nu}, \tag{9}$$

with L the length scale of a particle (here ESD) and ν the kinematic viscosity of the fluid (e.g. Dietrich, 1982).

2.2. Experiment validation

The experimental procedure was validated by measuring the size and w_s of certified polystyrene (PS, 1050 kg m^{-3}) spheres of 20, 40 and 100 µm diameter (Duke Standards, NIST Traceable Mean diameter, Thermo Fisher Scientific, Germany). The spheres were inserted into the cuvette at the beginning of experimental runs and were visually distinguished from sample particles in shadowgraphs.

The experimental setup is prone to occasionally produce erroneous w_s of a sphere due to water turbulence that cannot be detected from the sequence image, resulting in unrealistically high variability of results (Glockzin et al., 2014). Sinking velocities of PS spheres were grouped by the sphere's nominal size and the salinity of the experimental water, and results were identified as outliers if they lay outside 1.5 times the interquartile range of the group's sinking velocities, i.e. outside the whiskers of a (common) box plot. Out of 403 validation values, 16 were removed, suggesting that < 4% of all measurements deviate significantly from the particle's undisturbed terminal sinking velocity.

Results and meta data of the experiment validation are summarized in Table 1. The measured size of the PS spheres deviates slightly from their certified values, with 19.99 ± 0.25, 39.94 ± 0.35, and 100 ± 1.5 µm spheres having mean ESDs of 21 ± 1.2, 40.52 ± 1.99, and 99.39 ± 1.42 µm, respectively. Deviation from certified sizes has been reported for this method before (e.g. Glockzin et al., 2014). The difference is due to the low resolution of the shadowgraphy images (768 × 1024 pixels) and the falloff of light at the edge of the sphere shadow, which prevent precise dimension measurements. One-sample t-tests indicate that this difference between the certified nominal sizes of calibration spheres and their measured sizes is statistically significant at $p \leq 0.001$. However, the small values of difference suggest that deviations between measured and actual size have a negligible effect on measurements of other particles, whose size is approximated by equivalent spherical diameter.

The w_s of certified spheres varied considerably around the mean for each nominal size, with the relative standard deviation ranging between 5 and 36%, similar to previously reported relative standard deviation for this method (Glockzin et al., 2014). The relationship between particle size and w_s for the particle size range relevant to this study was best approximated by a quadratic regression. Despite considerable standard deviation, the quadratic fit through the validation data shows good determination of w_s by ESD (Fig. 1). Adjusted R^2 for such a quadratic fit is 0.95 for salinity 0, 0.97 for salinity 15, and 0.79 for salinity 36. This shows that the experimental setup is able to reproduce 79 to 97% of the effect particle size exerts on w_s.

Given the terminal sinking velocities w_s shown in Table 1 and Fig. 1, and a kinematic viscosity ν of the fluid of 0.000001, the Reynolds number of calibration spheres in the experiment ranged from 0.00008 to 0.03, indicating a laminar flow regime, where Stokes' law applies. Measured sinking velocities of certified spheres are directly compared to theoretical terminal sinking velocities of perfect spheres calculated using Stokes Law (Fig. 1). Though not calculated as a quadratic dependency of w_s on size, w_s predicted via Stokes' law also closely follows a quadratic relationship to particle size at the scale applicable in the experiment (Fig. 1). Analysis of variance (ANOVA) was used to compare measured w_s to Stokes values for the same size of spheres. Measured and theoretical w_s were used as treatment factors in a combined model, in which w_s is a function of the quadratic size of the particle and the treatment factor. This dependency was modeled with interactions between size and treatment factor and repeated without interactions. An ANOVA run on the two iterations reveals that the interaction has a significant effect if the model with interactions is significantly different from the model without interactions. In the present case this means that the fitted models for measured w_s and Stokes w_s are significantly different. ANOVA p-values were < 0.001, < 0.001, and 0.24 for salinity 0, 15, and 36, respectively. This suggests that the experiment produces reliable results throughout the tested particle size range at salinity 36 but may somewhat underestimate w_s of particle > 50 µm at salinity 0 and 15.

Results of PS sphere sinking measurements were also used to test the effect of slight temperature variability during the experiments. During validation, the average temperature was 19.6 °C, with a range of 18.6 to 20.4 °C. No combination of sphere size and salinity showed significant correlation of w_s with water temperature, indicating that density and viscosity changes caused by variability in water temperature did not influence w_s of particles during the experiments.

3. Results and discussion

The experiment included a wide range of particle sizes, ESD of PA, PET, and PMMA particles ranged from 9 to 140 µm, 7 to 251 µm, and 6 to 101 µm, respectively. The terminal sinking velocity, w_s, of PA particles ranged from 0.91 to 17.97 m d^{-1} at salinity 0, from 0.58 to 117.68 m d^{-1} at salinity 15, and from 0.56 to 33.6 m d^{-1} at salinity 36. The ranges of w_s for PET were 1.12–19.1, 0.9–88.54, and 1.52–38.74 m d^{-1} at salinity 0, 15, and 36, respectively. The w_s of PMMA particles at these respective salinities was 0.42–20.82, 0.72–23.31, and 0.57–35.33 m d^{-1}.

The Reynolds number Re was consistently ≪1, indicating a laminar flow regime during experiments.

As the relationship between particle size (< 1 mm) and w_s is well described by a quadratic function (compare Section "2.2. Experiment validation"), quadratic models were fitted using a least squares method to describe this relationship for the irregularly shaped sub-mm microplastic used in this experiment (Fig. 2). Coefficients for the quadratic linear dependency

$$w_s = \beta_0 + \beta_1 ESD + \beta_2 ESD^2$$

are given in Table 2. A quadratic fit generally yielded a higher determination coefficient than a linear fit, though the difference was small in most cases. The p-value adjusted R^2 for w_s as a quadratic function of size (ESD) at salinities 0, 15 and 36, respectively, was 0.66, 0.62, and

Table 1
Summary results of experiment validation by sinking of certified PS spheres.

Salinity	Diameter [µm]	N	T [°C]	T SD	ESD [µm]	ESD SD	w_s [m/d]	w_s SD	Stokes [m/d]	Stokes SD
0	20	28	19.82	0.05	22.07	0.66	1.52	0.39	1.18	0.07
0	40	33	19.91	0.21	42.36	2.76	4.37	1.40	4.36	0.54
0	100	25	19.62	0.25	99.68	1.07	18.87	2.52	24.02	0.51
15	20	55	19.36	0.08	20.73	1.04	0.62	0.03	0.79	0.08
15	40	38	18.91	0.10	40.02	0.55	3.64	1.09	2.93	0.08
15	100	56	19.00	0.42	99.50	1.63	16.90	1.73	18.10	0.59
36	20	27	20.21	0.14	20.55	1.34	0.77	0.28	0.45	0.06
36	40	43	20.22	0.12	39.54	0.84	1.88	0.44	1.66	0.07
36	100	75	19.90	0.26	99.35	1.41	11.44	3.52	10.47	0.30

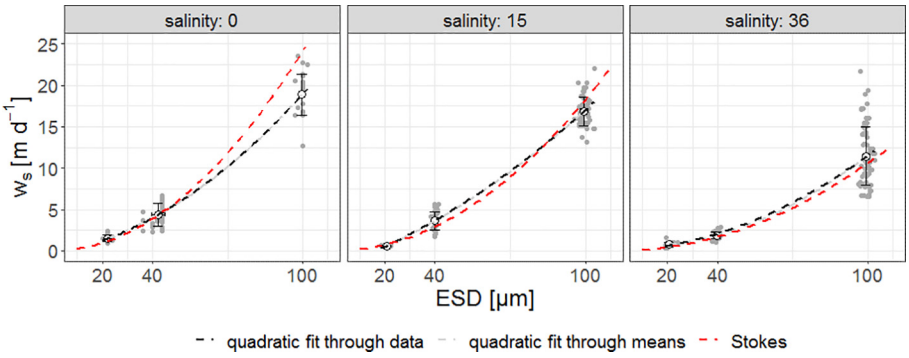

Fig. 1. Terminal sinking velocity w_s of different sized PS calibration spheres. Grey dots are original data, white dots with error bars are means ± one standard deviation. Black dashed line is the quadratic fit through all sample values (grey dots), grey dashed line is the quadratic fit through the means (black circles). The red dashed line represents the theoretical w_s according to Stokes (1845). (For interpretation of the references to color in this figure legend, the reader is referred to the web version of this article.)

0.21 for PA, 0.82, 0.75, and 0.51 for PET, and 0.83, 0.67, and 0.61 for PMMA.

Fig. 2 also shows terminal sinking velocities predicted for perfect spheres and ellipsoid particles using formulae by Stokes (1845) and Dietrich (1982), and Komar (1980), respectively, as well as for natural grains using approximations by Ahrens (2000) and Zhiyao et al. (2008). Measured values deviate considerably from theoretical values, with the quadratic fit curves of w_s generally below values predicted by Stokes (1845), Dietrich (1982), Komar (1980) and Ahrens (2000). The approximation by Ahrens (2000) has been shown to most precisely predict w_s for microplastic of different regular shapes in a size range of 0.59–6.23 mm (Khatmullina and Isachenko, 2017). In the size range of particles used in the present experiment however, the approximation by Ahrens yields virtually the same values as those by Stokes, Dietrich (for spheres) and Komar. The irregular shape of a particle implies a larger surface to volume ratio than found for spheres of the same ESD, causing higher pressure and friction drag (e.g. Dietrich, 1982). Thus, the sinking velocities of irregularly shaped particles are expected to be lower than the theoretical velocities calculated for perfect spheres, which has been shown for natural and anthropogenic particles, including microplastic (Kumar et al., 2010; Glockzin et al., 2014; Chubarenko et al., 2016; Kowalski et al., 2016). In several cases measured w_s was higher than values expected from theoretical approximations. This was mostly true for smaller particles (Fig. 2). Experimental uncertainty is higher for smaller particles because the smaller size and consequent slower sinking result in shorter and less precise distance measurements at a given shadowgraphy image resolution compared to larger and faster particles. Furthermore, because the reduction of w_s caused by irregular

Table 2
Coefficients for the quadratic fit of w_s determined by particle size (ESD).

Polymer	Salinity	β_0	β_1	β_2
PA	0	0.1872	0.0450	0.0009
PA	15	3.3847	0.0110	0.0039
PA	36	7.1543	−0.0450	0.0024
PET	0	2.5102	−0.0145	0.0005
PET	15	−0.5173	0.1618	0.0006
PET	36	3.0610	0.1774	0.0002
PMMA	0	−0.4145	0.1025	0.0018
PMMA	15	3.6358	−0.1171	0.0041
PMMA	36	7.9432	−0.2663	0.0051

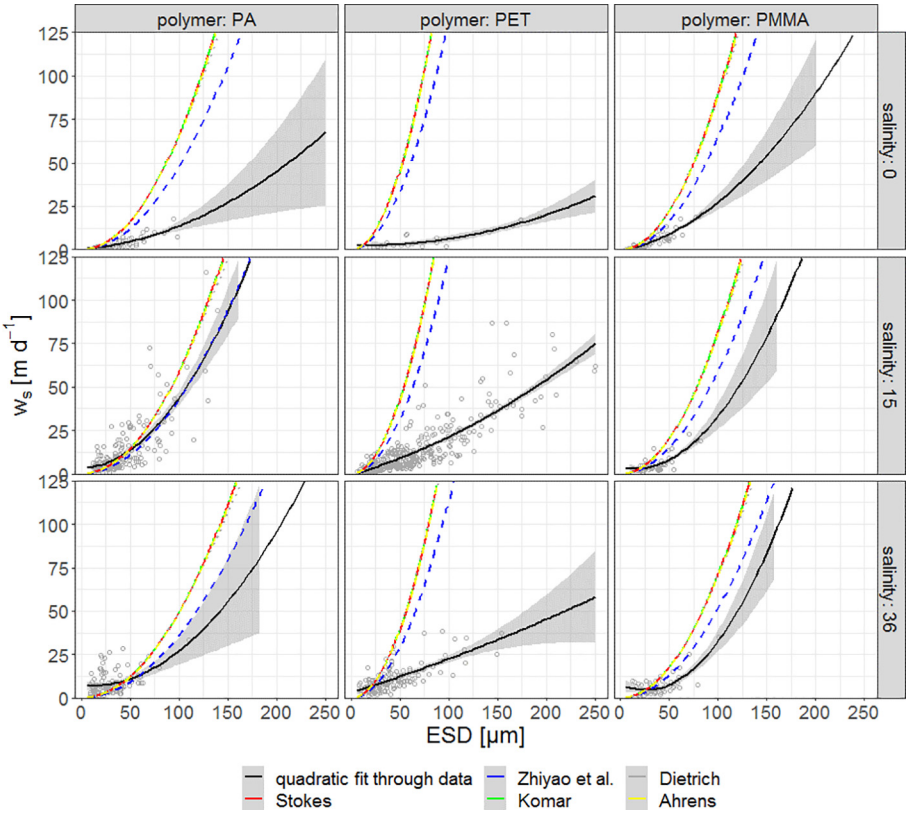

Fig. 2. Vertical sinking velocity of different sized irregularly shaped microplastic particles. The black line and grey shaded area are the quadratic fit through the data and its 95% confidence interval. The red and blue dashed lines represent the theoretical sinking velocity according to Stokes (1845) and Zhiyao et al. (2008), respectively. (For interpretation of the references to color in this figure legend, the reader is referred to the web version of this article.)

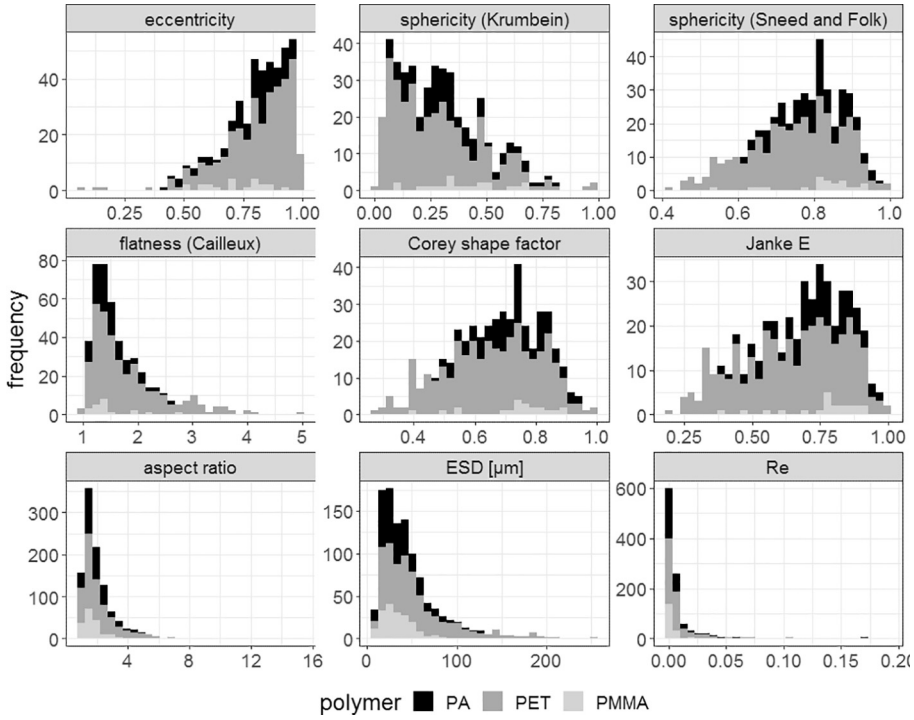

Fig. 3. Frequency distribution of shape characteristics of particles used in the sinking experiments. Calculations are described in the text. Values represent a subset of particles (compare text) except for aspect ratios (longest to shortest axis), ESD and Reynolds Number *Re*, which represent the entire set of particles.

Table 3
Median values of shape characteristics of particles used in the sinking experiments. Calculations are described in the text. Values represent a subset of particles (compare text) except for aspect ratios (longest to shortest axis), which represent the entire set of particles.

Variable	PA	PET	PMMA
Eccentricity	0.82	0.85	0.71
Sphericity (Krumbein, 1941)	0.30	0.23	0.37
Sphericity (Sneed and Folk, 1958)	0.81	0.76	0.83
Flatness (Cailleux, 1945)	1.41	1.61	1.36
Corey shape factor (Komar, 1980)	0.73	0.66	0.76
Janke E (Komar, 1980)	0.75	0.67	0.78
Aspect ratio	1.75	1.80	1.60

shape increases with particle size (Komar and Reimers, 1978), the effect of experimental uncertainty is especially important for smaller particles. This may explain why at small ESD (generally < 25 µm) both the measured sinking velocity and the quadratic model fit through those values are sometimes higher than theoretical velocity.

The calculation of w_s by Zhiyao et al. (2008) is based on a semi-empirical equation established for a wide range of particle sizes and shapes, not only small spheres, and hence yields lower velocities than Stokes' law (Fig. 3). While w_s of irregularly shaped microplastic particles more closely approach these estimates, they remain considerably lower (Fig. 3), indicating that the formula by Zhiyao et al. (2008) is not appropriate to predict w_s of microplastic with characteristics such as those used in this experiment. The deviation from w_s calculated for spheres of equivalent size was stronger for PET than PA and PMMA (Fig. 2). According to polymer densities, PET (1390 kg m^{-3}) should exhibit a steeper increase in w_s with ESD compared to PA (1140 kg m^{-3}) and PMMA (1190 kg m^{-3}), while during the experiments the increase was less strong for PET than PA and PMMA. Such discrepancies have been described for microplastic particles > 0.3 µm by Kowalski et al. (2016), who found higher sinking velocity for PA than PVC (with a density of 1560 kg m^{-3}), and attributed the discrepancy to the shape of the particles. The effect of shape on w_s is corroborated by comparing results of irregularly shaped particles and PS spheres. The modeled w_s of PS spheres more closely approaches theoretical values and has generally higher determination coefficients for the effect of size on w_s (0.79–0.97) than is the case for irregularly shaped particles (0.21–0.83). Both phenomena reflect that in addition to experimental uncertainty, deviation from theoretical w_s is caused by particles characteristics.

The statistical distribution of shape characteristics of these sub-mm particles is given in Fig. 3 and summarized in Table 3. Example shadowgraphs displaying the variability in particle shape and size are shown in Fig. S1 in electronic Supplementary material. The shape irregularity, i.e. deviation from spherical shape, was strongest for PET, which had lower sphericity and shape factor values but higher aspect ratio, eccentricity and flatness (Table 3). This explains the stronger non-spherical sinking behavior of PET seen in Fig. 2.

In order to arrive at a more generalized approximation that predicts w_s not only for specific combinations of plastic polymer (i.e. particle density) and salinity (i.e. fluid density, given fixed temperature), w_s can be expressed as a function of particle size (ESD) and particle excess density (Δρ = particle density minus fluid density).

The dependency of w_s on particle size was expressed as a quadratic regression, in accordance with results shown in Fig. 2. To determine the best prediction of w_s from Δρ, we fitted regressions with increasing polynomal degrees and used ANOVA to determine which raise of polynomial degree results in a significant reduction of the residual sum of squares. For the first instance in which a raise in polynomial degree did not significantly reduce the residual sum of squares, the higher complexity of the regression was deemed not useful. This procedure revealed that the dependency of w_s on particle excess density is also best described by a quadratic regression.

According to these results, a multiple quadratic regression predicts the terminal sinking velocity as a function of particle size and particle excess density as:

$$w_s = 11.68 + 0.1991 * ESD + 0.0004 * ESD^2 - 0.0993 * \Delta\rho + 0.0002 * \Delta\rho^2 \quad (10)$$

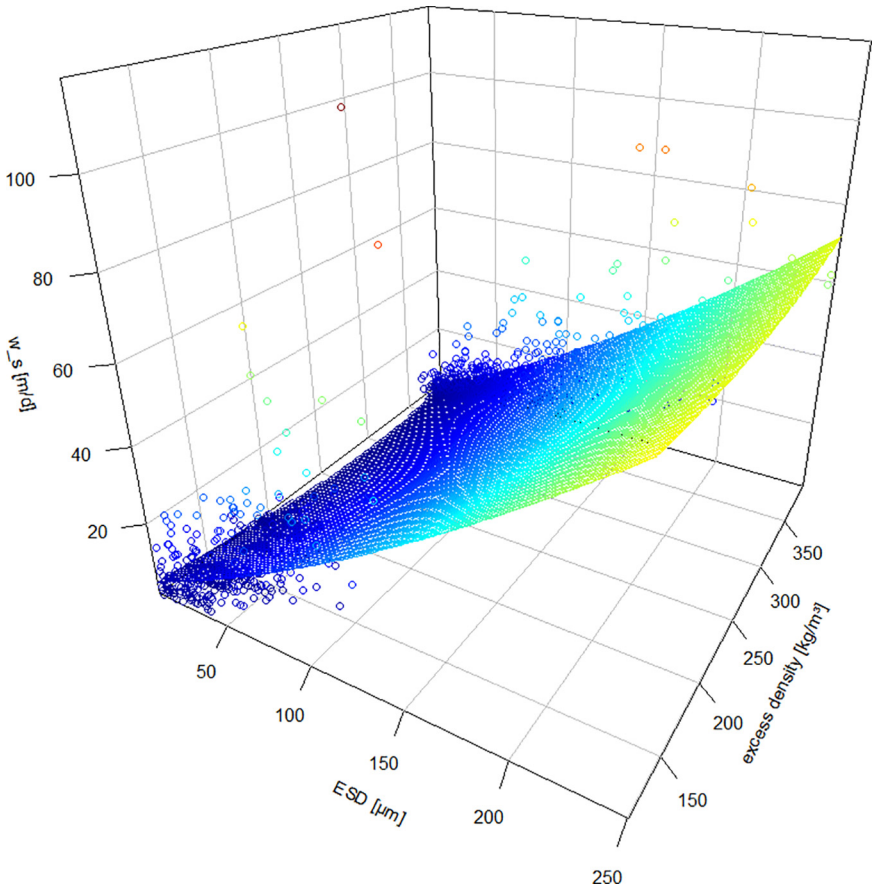

Fig. 4. Terminal sinking velocity as a function of particle size and particle density excess.

This relationship is graphically shown in Fig. 4, together with the results of the experiment. All coefficients are statistically significant at $p \leq 0.05$, and the regression has an adjusted $R^2 = 0.58$, indicating that the model explains 58% of the variability in particle terminal sinking velocity.

The accuracy of the prediction, expressed as the average relative error

$$E = \frac{1}{N}\Sigma_{i=1}^{N}\frac{predicted\ w_{s_i}}{measured\ w_{s_i}} - 1, \tag{11}$$

with N the number of measurements, takes a value of 47%.

The experimental results can also be expressed in terms of the dimensionless size W_* and dimensionless sinking velocity W_* defined by Dietrich (1982) as

$$D_* = \frac{(\rho_s - \rho)gD_n^3}{\rho\nu^2} \tag{12}$$

and

$$W_* = \frac{\rho w_s^3}{(\rho_s - \rho)g\nu}, \tag{13}$$

where ρ_s is the density of a particle with the nominal diameter D_n (here ESD), ρ and ν are the fluid density and kinematic viscosity, and g is gravity.

The relationship of W_* as a function of D_* has an adjusted R^2 of 0.38, considerably lower than the determination coefficient of Eq. (10) shown in Fig. 4, making it a weaker predictor of terminal sinking velocity.

4. Conclusion

This study provides the first empirical results of terminal sinking velocity w_s of irregularly shaped microplastic particles < 1 mm. As expected from particle sinking theory, w_s is lower than expected for similarly sized spheres. Tested available approximations of sinking velocity did not well represent the measured w_s. A new multiple quadratic regression model offers the possibility to predict about 60% of the variability of w_s for irregulary shaped microplastic as a functin of particle size and excess density over the surrounding fluid.

This should aid the prediction or reconstruction of sub-mm microplastic particle transport through the aquatic environment. For instance, an irregularly shaped microplastic particle with a density of 1050 kg m^{-3} and a nominal diameter of 50 µm sinking through a water column of 5000 m depth with an average temperature of 5.6 °C and an average salinity of 35.4 would need 234 days to reach the seafloor. Of course, numerous factors influence the effective time of vertical particle transport in the environment, and those must be addressed in future studies. Necessary improvements to the predictive power of the presented model require additional experiments with a wide range of particle characteristics. Parameters not addressed in this study might exert some effect on the sinking velocity, including e.g. the particle's surface roughness.

Supplementary data to this article can be found online at https://doi.org/10.1016/j.marpolbul.2018.12.035.

Acknowledgments

The authors wish to thank J. Markowski (BTU Cottbus) for the preparation of the polymer particles used in the experiments. This work is part of the MikrOMIK project which is funded by the Leibniz

Association (WGL 2014-2017). The authors thank M. Labrenz and S. Oberbeckmann (IOW) for project management and coordination. During the preparation of this article DK was financed by BMBF (project number 03F0786A). We gratefully acknowledge detailed and constructive comments from three reviewers on a previous version of this paper.

References

Ahrens, J.P., 2000. A fall-velocity equation. J. Waterw. Port Coast. Ocean Eng. 126 (2), 99–102. https://doi.org/10.1061/(ASCE)0733-950X(2000)126:2(99).

Bagaev, A., Mizyuk, A., Khatmullina, L., Isachenko, I., Chubarenko, I., 2017. Anthropogenic fibres in the Baltic Sea water column: field data, laboratory and numerical testing of their motion. Sci. Total Environ. 599–600, 560–571. https://doi.org/10.1016/j.scitotenv.2017.04.185.

Baldock, T.E., Tomkins, M.R., Nielsen, P., Hughes, M.G., 2004. Settling velocity of sediments at high concentrations. Coast. Eng. 51 (1), 91–100. https://doi.org/10.1016/j.coastaleng.2003.12.004.

Bellas, J., Martínez-Armental, J., Martínez-Cámara, A., Besada, V., Martínez-Gómez, C., 2016. Ingestion of microplastics by demersal fish from the Spanish Atlantic and Mediterranean coasts. Mar. Pollut. Bull. 109, 55–60. https://doi.org/10.1016/j.marpolbul.2016.06.026.

Browne, M.A., Dissanayake, A., Galloway, T.S., Lowe, D.M., Thompson, R.C., 2008. Ingested microscopic plastic translocates to the circulatory system of the mussel, *Mytilus edulis* (L.). Environ. Sci. Technol. 42, 5026–5031. https://doi.org/10.1021/es800249a.

Browne, M.A., Galloway, T.S., Thompson, R.C., 2010. Spatial patterns of plastic debris along estuarine shorelines. Environ. Sci. Technol. 44, 3404–3409. https://doi.org/10.1021/es903784e.

Cailleux, A., 1945. Distinction des galets marins et fluviatiles. Soc. Geol. Fr. Bull. 15, 375–404. https://doi.org/10.2113/gssgfbull.S5-XV.7-8.375.

Camenen, B., 2007. Simple and General Formula for the Settling Velocity of Particles. J. Hydraul. Eng. 133 (2), 229–233. https://doi.org/10.1061/(ASCE)0733-9429(2007)133:2(229).

Cheng, N.S., 1997. Effect of concentration on settling velocity of sediment particles. J. Hydraul. Eng. 123 (8), 728–731. https://doi.org/10.1061/(ASCE)0733-9429(1997)123:8(728).

Chubarenko, I., Bagaev, A., Zobkov, M., Esiukova, E., 2016. On some physical and dynamical properties of microplastic particles in marine environment. Mar. Pollut. Bull. 108, 105–112. https://doi.org/10.1016/j.marpolbul.2016.04.048.

Claessens, M., Meester, S.D., Landuyt, L.V., Clerck, K.D., Janssen, C.R., 2011. Occurrence and distribution of microplastics in marine sediments along the Belgian coast. Mar. Pollut. Bull. 62, 2199–2204. https://doi.org/10.1016/j.marpolbul.2011.06.030.

Cole, M., Lindeque, P., Fileman, E., Halsband, C., Galloway, T.S., 2015. The impact of polystyrene microplastics on feeding, function and fecundity in the marine copepod *Calanus helgolandicus*. Environ. Sci. Technol. 49, 1130–1137. https://doi.org/10.1021/es504525u.

da Costa, J.P., Santos, P.S.M., Duarte, A.C., Rocha-Santos, T., 2016. (Nano)plastics in the environment – sources, fates and effects. Sci. Total Environ. 566–567, 15–26. https://doi.org/10.1016/j.scitotenv.2016.05.041.

Courtene-Jones, W., Quinn, B., Gary, S.F., Mogg, A.O.M., Narayanaswamy, B.E., 2017. Microplastic pollution identified in deep-sea water and ingested by benthic invertebrates in the Rockall Trough, North Atlantic Ocean. Environ. Pollut. 231, 271–280. https://doi.org/10.1016/j.envpol.2017.08.026.

Cózar, A., Echevarria, F., Gonzalez-Gordillo, J.I., Irigoien, X., Ubeda, B., Hernandez-Leon, S., Palma, A.T., Navarro, S., Garcia-de-Lomas, J., Ruiz, A., Fernandez-de-Puelles, M.L., Duarte, C.M., 2014. Plastic debris in the open ocean. Proc. Natl. Acad. Sci. 111, 10239–10244. https://doi.org/10.1073/pnas.1314705111.

Cózar, A., Sanz-Martín, M., Martí, E., González-Gordillo, J.I., Ubeda, B., Gálvez, J.Á., Irigoien, X., Duarte, C.M., 2015. Plastic accumulation in the Mediterranean Sea. PLoS One 10, e0121762.

Desforges, J.-P.W., Galbraith, M., Dangerfield, N., Ross, P.S., 2014. Widespread distribution of microplastics in subsurface seawater in the NE Pacific Ocean. Mar. Pollut. Bull. 79, 94–99. https://doi.org/10.1016/j.marpolbul.2013.12.035.

Dietrich, W.E., 1982. Settling velocity of natural particles. Water Resour. Res. 18, 1615–1626.

Doyle, M.J., Watson, W., Bowlin, N.M., Sheavly, S.B., 2011. Plastic particles in coastal pelagic ecosystems of the Northeast Pacific ocean. Mar. Environ. Res. 71 (1), 41–52. https://doi.org/10.1016/j.marenvres.2010.10.001.

Fischer, V., Elsner, N.O., Brenke, N., Schwabe, E., Brandt, A., 2015. Plastic pollution of the Kuril–Kamchatka Trench area (NW Pacific). Deep Sea Res. Part II Top. Stud. Oceanogr. 111, 399–405. https://doi.org/10.1016/j.dsr2.2014.08.012.

Glockzin, M., Pollehne, F., Dellwig, O., 2014. Stationary sinking velocity of authigenic manganese oxides at pelagic redoxclines. Mar. Chem. 160, 67–74. https://doi.org/10.1016/j.marchem.2014.01.008.

Gregory, M.R., 1996. Plastic "scrubbers" in hand cleansers: a further (and minor) source for marine pollution identified. Mar. Pollut. Bull. 32, 867–871. https://doi.org/10.1016/S0025-326X(96)00047-1.

Hidalgo-Ruz, V., Gutow, L., Thompson, R.C., Thiel, M., 2012. Microplastics in the marine environment: a review of the methods used for identification and quantification. Environ. Sci. Technol. 46, 3060–3075. https://doi.org/10.1021/es2031505.

Kanhai, L.D.K., Gårdfeldt, K., Lyashevska, O., Hassellöv, M., Thompson, R.C., O'Connor, I., 2018. Microplastics in sub-surface waters of the Arctic Central Basin. Mar. Pollut. Bull. 130, 8–18. https://doi.org/10.1016/j.marpolbul.2018.03.011.

Khatmullina, L., Isachenko, I., 2017. Settling velocity of microplastic particles of regular shapes. Mar. Pollut. Bull. 114 (2), 871–880. https://doi.org/10.1016/j.marpolbul.2016.11.024.

Komar, 1980. Settling velocities of circular cylinders at low Reynolds numbers. J. Geol. 88 (3), 327–336. https://doi.org/10.1086/628510.

Komar, P.D., Reimers, C.E., 1978. Grain shape effects on settling rates. J. Geol. 86, 193–209. https://doi.org/10.1086/649674.

Kooi, M., Besseling, E., Kroeze, C., van Wezel, A.P., Koelmans, A.A., 2018. Modeling the fate and transport of plastic debris in freshwaters: review and guidance. In: Wagner, M., Lambert, S. (Eds.), Freshwater Microplastics. Springer International Publishing, Cham, pp. 125–152. https://doi.org/10.1007/978-3-319-61615-5_7.

Kowalski, N., Reichardt, A.M., Waniek, J.J., 2016. Sinking rates of microplastics and potential implications of their alteration by physical, biological, and chemical factors. Mar. Pollut. Bull. https://doi.org/10.1016/j.marpolbul.2016.05.064.

Krumbein, W.C., 1941. Measurement and geological significance of shape and roundness of sedimentary particles. J. Sediment. Petrol. 11 (2), 64–72. https://doi.org/10.1306/D42690F3-2B26-11D7-8648000102C1865D.

Kumar, R.G., Strom, K.B., Keyvani, A., 2010. Floc properties and settling velocity of San Jacinto estuary mud under variable shear and salinity conditions. Cont. Shelf Res. 30, 2067–2081. https://doi.org/10.1016/j.csr.2010.10.006.

Lenz, R., Enders, K., Nielsen, T.G., 2016. Microplastic exposure studies should be environmentally realistic. Proc. Natl. Acad. Sci. 113, E4121–E4122. https://doi.org/10.1073/pnas.1606615113.

Liubartseva, S., Coppini, G., Lecci, R., Clementi, E., 2018. Tracking plastics in the Mediterranean: 2D Lagrangian model. Mar. Pollut. Bull. 129, 151–162. https://doi.org/10.1016/j.marpolbul.2018.02.019.

Moore, C.J., Moore, S.L., Leecaster, M.K., Weisberg, S.B., 2001. A comparison of plastic and plankton in the North Pacific central gyre. Mar. Pollut. Bull. 42, 1297–1300.

Ristow, G.H., 1997. Wall correction factor for sinking cylinders in fluids. Phys. Rev. E 55, 2808.

Sneed, E.D., Folk, R.L., 1958. Pebbles in the lower Colorado River, Texas—a study of particle morphogenesis. J. Geol. 66, 114–150. https://doi.org/10.1086/626490.

Stokes, G.G., 1845. On the theories of the internal friction of fluids in motion and of the equilibrium and motion of elastic solids. Trans. Camb. Philos. Soc. 8, 287–319.

Sutton, R., Mason, S.A., Stanek, S.K., Willis-Norton, E., Wren, I.F., Box, C., 2016. Microplastic contamination in the San Francisco Bay, California, USA. Mar. Pollut. Bull. 109, 230–235. https://doi.org/10.1016/j.marpolbul.2016.05.077.

Thompson, R.C., Swan, S.H., Moore, C.J., vom Saal, F.S., 2009. Our plastic age. Philos. Trans. R. Soc. B Biol. Sci. 364, 1973–1976. https://doi.org/10.1098/rstb.2009.0054.

Van Cauwenberghe, L., Janssen, C.R., 2014. Microplastics in bivalves cultured for human consumption. Environ. Pollut. 193, 65–70. https://doi.org/10.1016/j.envpol.2014.06.010.

Van Cauwenberghe, L., Devriese, L., Galgani, F., Robbens, J., Janssen, C.R., 2015. Microplastics in sediments: a review of techniques, occurrence and effects. Mar. Environ. Res. 111, 5–17. https://doi.org/10.1016/j.marenvres.2015.06.007.

Woodall, L.C., Sanchez-Vidal, A., Canals, M., Paterson, G.L., Coppock, R., Sleight, V., et al., 2014. The deep sea is a major sink for microplastic debris. R. Soc. Open Sci. 1, 140317. https://doi.org/10.1098/rsos.140317.

Zhang, H., 2017. Transport of microplastics in coastal seas. Estuar. Coast. Shelf Sci. 199, 74–86. https://doi.org/10.1016/j.ecss.2017.09.032.

Zhiyao, S., Tingting, W., Fumin, X., Ruijie, L., 2008. A simple formula for predicting settling velocity of sediment particles. Water Sci. Eng. 1, 37–43.